

A mobile kinesin-head intermediate during the ATP-waiting state

Ana B. Asenjo and Hernando Sosa¹

Department of Physiology and Biophysics, Albert Einstein College of Medicine, 1300 Morris Park Avenue, Bronx, NY 10461

Edited by Steven M. Block, Stanford University, Stanford, CA, and approved February 24, 2009 (received for review August 22, 2008)

Kinesin1 is a motor protein that uses the energy from ATP hydrolysis to move intracellular cargoes along microtubules. It contains 2 identical motor domains, or heads, that coordinate their mechano-chemical cycles to move processively along microtubules. The molecular mechanism of coordination between head domains remains unclear, partly because of the lack of structural information on critical intermediates of the kinesin1 mechano-chemical cycle. A point of controversy has been whether before ATP binding, in the so called ATP-waiting state, 1 or 2 motor domains are bound to the microtubule. To address this issue, here we use ensemble and single molecule fluorescence polarization microscopy (FPM) to determine the mobility and orientation of the kinesin1 heads at different ATP concentrations and in heterodimeric constructs with microtubule binding impaired in 1 head. We found evidence for a mobile head during the ATP-waiting state. We incorporate our results into a model for kinesin translocation that accounts well for many reported experimental results.

cytoskeleton | fluorescence | microtubule | single-molecule | polarization

Kinesin1 is a motor protein that uses the energy of ATP hydrolysis to generate force and movement along microtubules (1). It contains 2 identical motor domains or heads where microtubule binding and ATP hydrolysis occur. It takes 8-nm steps between binding sites along the microtubule (2), hydrolyzing 1 ATP molecule per step (3–5). A stepping event is thought to occur when ATP binds to one of the heads inducing a disorder-to-order transition (docking) of a region called the neck linker, a short segment of ≈ 15 residues located at the C-terminal end of each head (6–8). Kinesin1 is a processive motor that can walk for more than a micrometer, going through hundreds of ATP hydrolysis cycles without dissociating from the microtubule (9). Processivity is achieved by an asymmetric hand-over-hand walking mechanism, in which the 2 heads coordinate their activities to alternate leading and trailing positions at each step (10–13).

The molecular mechanism of coordination between kinesin1 motor domains is still unclear. Kinetic studies have identified ADP release and nucleotide binding as one of the coordinating steps. In solution, kinesin1 binds ADP tightly and interaction with the microtubule results in rapid release of 1 ADP molecule per kinesin head dimer. The second ADP molecule is released much more slowly, unless there is ATP present (or a nonhydrolyzable ATP analogue) that accelerates the release of the second ADP molecule (14–16). This phenomenon constitutes a coordinating step or gate, as 1 kinesin head has to wait for the partner head to complete a particular step (ATP binding) to proceed (17). Several possible models have been proposed to explain this coordinating gate (18). One model proposes that in the ATP-waiting state the ADP containing head is kept away from the microtubule by interactions with the microtubule-bound head (19). Another model proposes that both motor domains can bind to the microtubule simultaneously but display distinct kinetics because the neck-linker elements connecting both heads are oppositely oriented (20, 21). To distinguish between these models, structural information of the configuration of the 2 kinesin1 heads is needed. FPM provided evidence that at

satürating ATP both motor domains spend most of the time bound to the microtubule (20), but it is not clear whether this configuration is also maintained at limiting concentrations of ATP when the molecule spends most of the time in the ATP-waiting state. Recent single molecule fluorescence resonance energy transfer (FRET) measurements have provided evidence for a one-head-only microtubule-bound intermediate in the ATP-waiting state (21). However, distance FRET measurements alone cannot distinguish whether the microtubule-unbound (tethered) head is kept away from the microtubule in a stable configuration or whether it is free to move by diffusion around the tether point. To address this issue we use fluorescence polarization microscopy (FPM) of ensemble and single molecules to determine the mobility and orientation of the kinesin1 heads when 1 head is unable to bind to the microtubule and during processive walking at limiting ATP concentrations. Our results indicate that in the ATP-waiting state 1 motor domain is mobile, and we found no evidence for a stable configuration different from the microtubule-bound one.

Results

The Tethered Motor Domain Does Not Have A Preferred Orientation.

To investigate the configuration of the kinesin motor domains when 1 head is microtubule bound and the other is unbound (tethered), we used heterodimeric kinesin1 constructs (22) with 1 head unable to bind the microtubule. One of the heads contains the triple mutation Y274A, R278A, and K281A in loop-12 (L12), which severely reduces microtubule binding in all nucleotide conditions (23). For site-specific labeling, all exposed cysteines were replaced by alanines or serines (cys-light). The constructs used are based on similar ones used recently to investigate the distances between motor domains using FRET (21). For FPM, we labeled the construct with the bifunctional probe BSR (*Methods*) at unique cysteines located at residues 64 and 71 (residues numbered according to KIF5B sequence) of either of the 2 motor domains (with or without L12 mutation). We named the 2 heterodimeric constructs created as wtBSR/L12 and L12BSR/wt to indicate respectively whether the BSR probe is in the unmodified (wt) or the mutated L12 motor domain (Fig. 1A). wtBSR/L12 reports on the configuration of the microtubule-bound motor domain, and L12BSR/wt reports on the tethered one. We also created a BSR-labeled homodimeric version of the constructs, without the L12 triple mutation, and named it wtBSR/wt. When the BSR labeled head is strongly bound to the microtubule, we would expect the BSR transition dipole probe to be oriented nearly parallel to the microtubule axis (Fig. 1B).

Ensemble FPM data with the 3 labeled constructs was obtained in the absence of nucleotides (NN) or in the presence of

Author contributions: A.B.A. and H.S. designed research; A.B.A. performed research; A.B.A. and H.S. analyzed data; and H.S. wrote the paper.

The authors declare no conflict of interest.

This article is a PNAS Direct Submission.

¹To whom correspondence should be addressed. E-mail: hsosa@aecom.yu.edu.

This article contains supporting information online at www.pnas.org/cgi/content/full/0808355106/DCSupplemental.

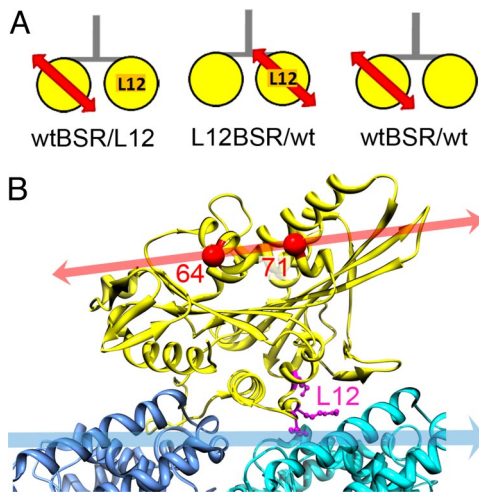


Fig. 1. Kinesin constructs and probe location. (A) Diagram of the 3 dimeric kinesin constructs used. The heterodimeric constructs wtBSR/L12 and L12BSR/wt have 1 BSR-labeled head (red arrow) and 1 head with the triple L12 mutation (L12). The homodimeric construct wtBSR/wt has no L12 mutation, and $\approx 87\%$ of the labeled protein has only 1 BSR label (*Methods*). (B) Ribbon representation of the kinesin motor domain bound to the microtubule in a strong bound state according to cryo-em data (36). The CB atoms of residues 64 and 71 where the BSR probe is attached are indicated by the red spheres, and the resulting orientation of the attached fluorescent transition dipole is indicated by the red arrow. The direction of the long microtubule axis is indicated by the blue arrow. The location of the L12 residues mutated to affect microtubule binding are indicated in magenta.

the nonhydrolysable ATP analogue, AMP-PNP. Both conditions induce strong binding of kinesin to microtubules (24). The results are summarized in Fig. 2 and [supporting information \(SI\) Fig. S1](#). When the probe is in the kinesin head with normal microtubule binding ability, a decorated microtubule has strong fluorescence anisotropy ([Fig. S1A](#)). The microtubule becomes brighter when the excitation light is parallel to the microtubule axis as expected from the orientation of the probe relative to the microtubule ([Fig. 1B](#)). By measuring the difference in intensities, depending on the polarization direction, we estimated the LD^0 parameter for each experimental condition ([Fig. S1](#)). The LD^0 is sensitive to the axial orientation of the fluorophore relative to the microtubule long axis (β -angle) and the amount of deviation (disorder or mobility) from the average β -angle. Extreme possible values are 1 and -1 indicating, respectively nonmobile probes completely perpendicular ($\beta = 90^\circ$) or parallel ($\beta = 0^\circ$) to the microtubule axis. An LD^0 value of zero corresponds to randomly oriented probes or probes oriented relative to the

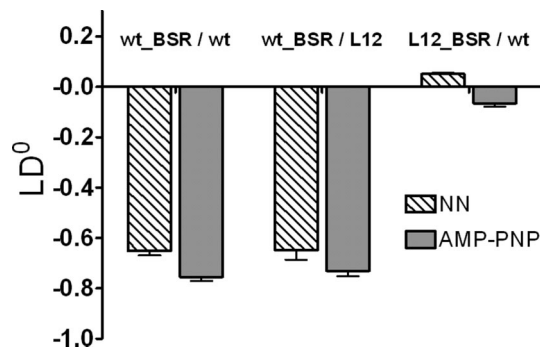


Fig. 2. Ensemble fluorescence polarization microscopy (FPM) bar plot of the calculated LD^0 values. Error bars represent the SE of the estimated LD^0 value. For details see [Fig. S1](#).

microtubule with $\beta = 54.7^\circ$ (25). The LD^0 values for the construct wtBSR/L12 are negative and close to -1 , indicating that the probes are well ordered and nearly parallel to the microtubule axis, as expected when a kinesin head is strongly bound to the microtubule ([Fig. 1B](#)). The values in the presence of AMP-PNP are slightly closer to -1 , suggesting even less mobility in this condition. The LD^0 values for the wtBSR/L12 and the wtBSR/wt constructs are very similar, indicating that both kinesin heads (leading or trailing) in the wtBSR/wt construct have a configuration similar to the microtubule-bound head of the wtBSR/L12 construct. This result is similar to the one reported in previous work which compared monomeric and dimeric constructs and reinforces the conclusion that in the AMP-PNP and non-nucleotide states, both kinesin1 heads are microtubule bound (20). In contrast to the constructs discussed above, the construct L12BSR/wt has LD^0 values close to zero in both nucleotide conditions, indicating that when the kinesin head is prevented from binding to the microtubule, it remains mobile. To distinguish the contributions of mobility and orientation, we analyzed single molecule FPM data ([Fig. 3](#) and [Table 1](#)). Examples of single molecule kymographs and intensity records are shown in [Fig. 3A](#) and [B](#), respectively. From the measured fluorescence anisotropies, we calculated for each molecule an order r -factor and the projected angle (PA) relative to the microtubule axis. Low r -factor values, closer to zero, indicate high mobility, whereas high r -factor values closer to 1 indicate order (25). To a first approximation, the peak of the PA distribution is close to the axial angle (β) between the probe dipole and the microtubule axis (7, 20). [Fig. 3C](#) and [D](#) shows, respectively the r -factor and PA frequency distributions derived from many individual single-molecule measurements in each experimental condition. The distributions corresponding to the wtBSR/L12 construct (red lines) are strongly skewed toward high r -factors and PA angles closer 0 (peak at $\approx 15^\circ$), as expected from the configuration of the kinesin1 head when strongly bound to the microtubule ([Fig. 1B](#)). In contrast, the distributions corresponding to the L12BSR/wt construct (blue lines in [Fig. 3C](#) and [D](#)) are skewed toward low r -factors and have no preferential PA angle, indicating a high degree of mobility. Thus, the ensemble and single molecule data show that a tethered kinesin head has no preferential orientation and is very mobile.

Nucleotide Binding Alters the Configuration of the Tethered Motor Domain. We detected small differences in the FPM data of the L12BSR/wt construct depending on the presence nucleotide. The difference is most evident in the ensemble FPM data where the measurements of higher fluorescence intensities and ensemble averaging results in higher signal to noise. The LD^0 in the NN condition is slightly positive (0.05) and goes slightly negative (-0.06) in the presence of AMP-PNP ([Fig. 2](#)). The difference between these 2 LD^0 values was statistically significant ($P \ll 0.001$). The shift to a negative (but close to zero) LD^0 with AMP-PNP suggests that the tethered head, although very mobile, spends some time in a configuration with the probe parallel to the microtubule axis. One possible explanation for this result is that in the presence of AMP-PNP the tethered head binds transiently to the microtubule. Transient interactions with the microtubule in the AMP-PNP state may also result in a different average distance between heads relative to the NN conditions as reported by FRET measurements in a similar kinesin construct (21).

There Is a Tethered Mobile Motor Domain in the ATP-Waiting State. We obtained single molecule FPM data from wtBSR/wt constructs walking processively at different concentrations of ATP. If during the ATP-waiting state there is a mobile tethered head, then we would predict an increase in mobility (lower r -factors) as ATP becomes limiting. On the other hand, if both heads are

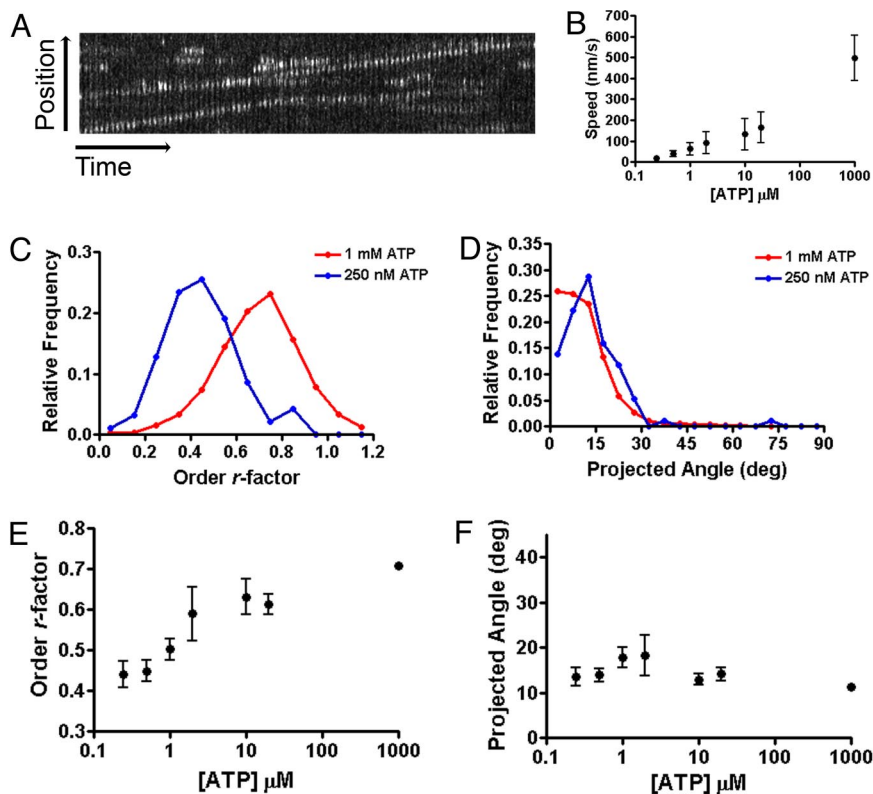


Fig. 4. Single molecule FPM of wtBSR/wt molecules walking in the presence of ATP. (A) Kymograph showing traces of single kinesin molecules walking in the presence of 1 mM ATP. (B) Average speed vs. [ATP]. Error bars: SD. (C) Time averaged order *r*-factor frequency distributions of walking kinesin molecules at [ATP] of 1 mM (red) and 250 nM (blue). (D) Time averaged projected angle (PA) distributions (colors and [ATP] as in C). Frequency distribution in C and D were built by calculating the average *r*-factor and projected angle during the whole observation interval of each molecule (Methods). In C and D, for clarity only the 2 distributions corresponding to the extremes of the ATP concentrations investigated are plotted. (E) Order *r*-factor vs. [ATP]. (F) Projected angle vs. [ATP]. In E and F, the points represent the distributions mean and the error bars the 95% CI.

parallel to the microtubule axis and the low *r*-factors periods coincide with variable angles. These 2 conditions are similar to the results with the heterodimeric constructs when the probe was located either in the microtubule-bound head or in the unable-to-bind tethered head (compare Fig. 5 B and C with Fig. 3 C and D). Therefore, the results with walking kinesins are consistent with a model in which each kinesin head alternates between a

nonmobile microtubule bound and a mobile tethered configuration during processive movement at limiting ATP (Fig. 5D).

The low and high mobility dwell lifetimes inversely correlate with the ATP concentration and the walking speed (Fig. 5D), strongly suggesting that the low and high mobility transitions are associated with the kinesin stepping mechanism. Furthermore, the average distance traveled per mobility transition (calculated

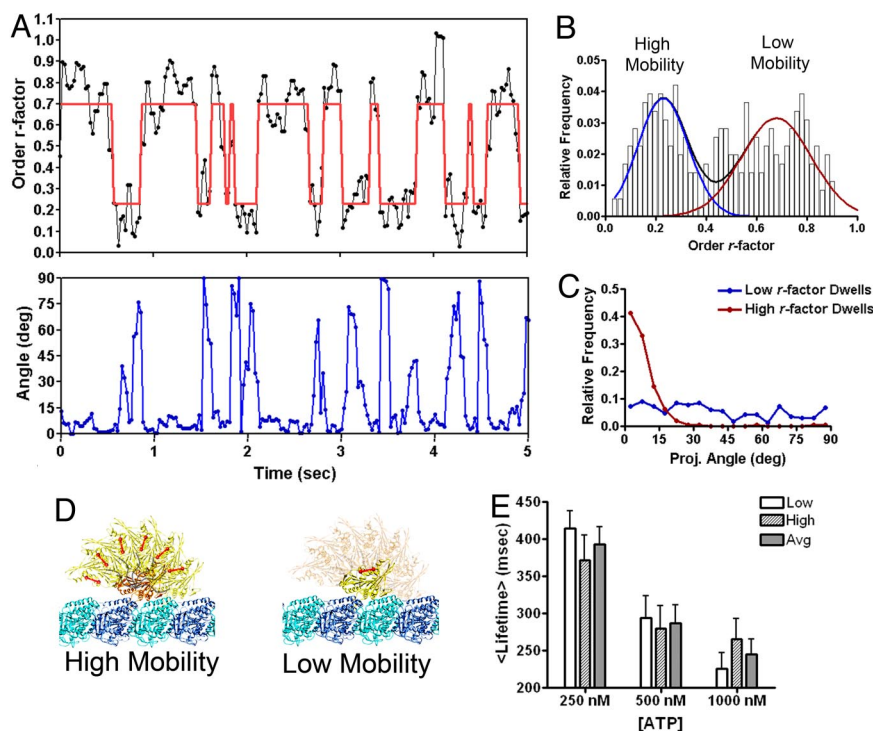


Fig. 5. Transitions between low and high mobility states in walking kinesins. (A) Time traces of order *r*-factor (Top) and projected angle (Bottom) of a molecule moving processively at 32 nm/sec in the presence of 500 nM [ATP]. In the top figure, the black line corresponds to the measured *r*-factors and the red line to the idealized values detected using a hidden Markov algorithm (35). For clarity only a 5-sec segment of the whole trace (8.9 sec) is shown. 39 events (low and high *r*-factor) were detected in this trace. (B) Time-resolved order *r*-factor distribution of the molecule shown in A. Total number of intensity measurements in the distribution is 356. (C) Time-resolved projected angle distribution corresponding to the high (red lines) and low (blue lines) *r*-factor dwells. (D) Interpretation of the *r*-factor transients. As the kinesin molecule walks, the motor domains alternate between high and low mobile states so the probe attached to one of the heads (red line) reports alternating low and high *r*-factors. (E) Average *r*-factor \langle lifetime \rangle vs. [ATP]. In each case the bars represent the average \langle lifetime \rangle of 9 molecules and the error bars the SE. The total number of events (low and high *r*-factor) detected in the 9 molecules analyzed in each case were 131, 181, and 228, respectively, for the 250, 500, and 1000 nM [ATP] conditions.

as the product $\langle \text{lifetime} \rangle \times \text{speed}$ for each molecule) at the lowest ATP concentrations investigated are close to the 8-nm kinesin stepping distance (7.5 ± 1.5 nm at 250 nM [ATP] and 9.9 ± 2.5 nm at 500 nM [ATP], mean \pm SD, $n = 9$ molecules in each case), indicating approximately 1 mobility transition per kinesin step. At ATP concentrations of 1 μ M and above the measured lifetimes are likely to be overestimated because of missing events caused by the limited time resolution of our set-up. At an average speed of 62 nm/sec (Table 1) the kinesin stepping $\langle \text{lifetime} \rangle$ would be 160 msec, which is below the 200-msec current time resolution of our FPM system (*Methods*).

Discussion

We have found evidence for a mobile kinesin1 head during the ATP-waiting state. In this state, 1 head is microtubule-bound, whereas the other is unbound or weakly bound with high mobility. This configuration is in contrast to the ones at saturating ATP, presence of AMP-PNP, or absence of nucleotides, where both heads are in a microtubule-bound configuration most of the time (20, 21). During the ATP-waiting state, the mobile tethered head containing ADP could transiently interact with the microtubule. This possibility would explain kinetic experiments indicating that microtubule interaction accelerates the rate of ATP resynthesis from ADP in the tethered head (26).

A model consistent with the FPM results and other data is shown in Fig. 6. In this model, both kinesin motor domains are tightly bound to the microtubule for most of the cycle, except in the short lived (at saturating ATP) ATP-waiting state. Two alternative configurations of the tethered head in the ATP-waiting state are considered (*Top* and *Bottom* inside the square in Fig. 6). Our data would be consistent with either one or a combination of both. In one alternative (*Top*), the tethered head is weakly bound to the microtubule and very mobile as has been previously described for a single motor domain in the presence of ADP (27). In the second alternative (*Bottom*), the tethered head is detached from the microtubule and very mobile. The first alternative is consistent with stepping distance measurements using FIONA indicating that each head takes alternate steps of similar size (12). The second alternative (*Bottom*) will better fit FRET measurements that indicate a shorter head-to-head distance in the ATP-waiting state relative to the situation when both heads are microtubule bound (21). A shorter head-to-head distance would be expected when 1 head detaches from the microtubule. If the neck linkers connecting the 2 motor domains behave as entropic springs (28) then their end-to-end distance would become shorter when undocked or not stretched between microtubule-bound motor domains. The reach distance of the tethered head would be determined by the restrictions imposed by the combined length of the neck linkers connecting the 2 heads. Exit from the ATP-waiting state would occur when ATP binds to the forward head, inducing neck linker docking (6–8). With a docked neck linker in the bound head, the tethered head could more easily reach and bind the next site on the microtubule. ADP is then released from the tethered head when it binds in the forward position. At this point, the kinesin molecule completes an 8-nm step.

In the above model, coordination between the 2 heads depends on the arrangement of kinesin binding sites on the microtubule lattice. Strain between the motor domains or the distinct orientation of the neck linkers on each motor domain provokes an asymmetry (20, 21, 29–31) so that ADP is released from the tethered head when it binds to the microtubule in the forward position but not in the trailing one. An alternative model for the ADP release gate, independent of the microtubule lattice, has been proposed based on the observation that the gate and tubulin binding can operate in the presence of free tubulin (19). In this model the tethered head is prevented from tubulin binding by occluding its binding site through interactions with

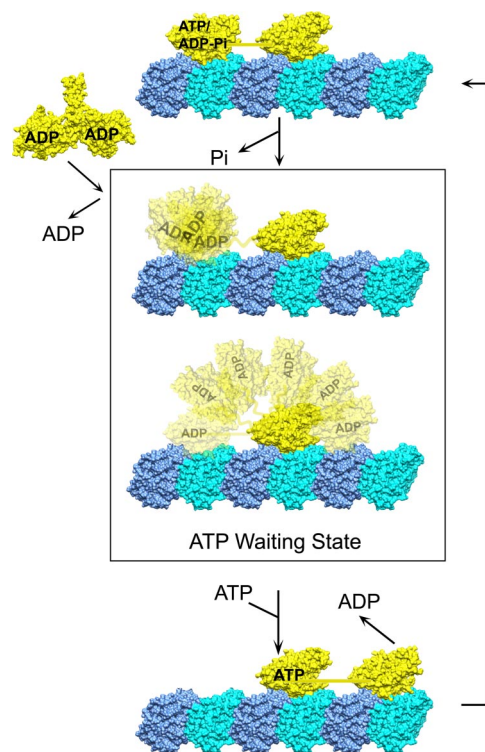


Fig. 6. Model for kinesin1 translocation. When a kinesin dimer containing 2 ADP molecule interacts with a microtubule for the first time, it releases 1 ADP molecule rapidly (14). The dimer then enters the ATP-waiting state with 1 mobile tethered head with ADP still bound to it. In this model, the nucleotide-free head is the leading one according to data indicating that nucleotide dissociation preferentially occurs in the forward-positioned head (29). Two possible configurations for the ATP-waiting state, consistent with our FPM data are shown. In the (*Top*) image, the tethered head is very mobile but remains weakly bound to the microtubule. In the (*Bottom*) image, the tethered head is detached from the microtubule. ATP binding to the microtubule-bound head docks its neck linker (6–8), allowing the tethered mobile head to reach the next microtubule binding site. At saturating ATP, the ATP-waiting state would be short lived relative to the whole cycle, and the 2 heads would be tightly bound to the microtubule most of the time (20). A full 8-nm step is completed between the start and end of the ATP-waiting state. For further discussion, see also *Discussion* section.

the other head. This model is harder to reconcile with our data. We found no evidence for a stable configuration of the tethered head, and a mobile head is likely to expose its tubulin binding site. Whether the tethered head is refractive to free tubulin binding by a mechanism other than hiding its binding site will require further investigation.

Materials and Methods

Protein Constructs. Kinesin constructs based on the human ubiquitous kinesin1 (Kif5b) sequence were prepared from DNA plasmids generously provided by M. Tomishige (University of Tokyo, Tokyo, Japan) and R. Vale (University of California, San Francisco, CA). The constructs contain Kif5b residues 1–490 with exposed cysteines replaced by alanines or serines (cys-light). Heterodimers were prepared by using a coexpression vector containing 2 kinesin sequences: one with a carboxy-terminal streptavidin tag (Strep-tag; 9 residues, AWRHPQFGG) and the other with a His₆ tag. DNA cloning was done according to ref. 8. The kinesin sequence with the His₆ also contained the triple mutation Y274A/R278A/K281A in L12 that inhibits microtubule binding (23). We also prepared a plasmid containing only the Strep-tagged kinesin sequence to make homodimers. Two unique cysteines were introduced at positions 64 and 71 of either of the 2 kinesin sequences for site-specific labeling with a bifunctional fluorescent probe.

Protein Purification and Labeling. Kinesin protein constructs were expressed in BL21 cells. The heterodimeric constructs were purified from lysates first by

nickel-nitrilotriacetic acid chromatography and then by Strep-Tactin (streptavidin mutant) affinity purification according to ref. 8. Purified kinesin constructs were labeled overnight with the bifunctional probe BSR according to refs. 7, 20. The heterodimeric constructs have only 1 pair of cysteines to be labeled with BSR in 1 of the heads. In the case of the homodimeric constructs, we estimated from the ratio of labeled to unlabeled protein and from single molecule fluorescence intensity records that $\approx 87\%$ of the labeled protein has the probe in only 1 head. The presence of the BSR probe cross-linking the 2 unique cysteines 64–71 in the proteins was verified by mass spectrometry. Protein preparations with $>10\%$ intermolecular cross-linked protein (as judged from SDS/PAGE) were further purified by gel filtration. According to cryo-em models of the kinesin-microtubule complex (36) the predicted axial angle between residues 64–71 β -carbons and the microtubule axis is 13° .

Sample Preparation. Positively charged coverslips with DETA were prepared according to ref. 32. Flow chambers were assembled by joining a DETA-treated coverslip and a nontreated coverslip using double stick tape. Microtubules were stuck to the flow chamber by flowing-in a solution with polymerized tubulin (10 $\mu\text{g/ml}$ tubulin, 80 mM Pipes, 1 mM EGTA, 2 mM MgCl_2 , 20 μM placitaxel, pH 6.8) and incubating for 5 min. Then solution A (7.5 mg/ml BSA, 2 mM MgCl_2 , 1 mM EGTA, 20 μM placitaxel, 12 mM Pipes, pH 6.8) plus an ATP regeneration system (2 mM PEP, 0.1 mg/ml Pyruvate kinase, Sigma Type III) (33), an anti-bleaching system (2.5 mM protocatechuic acid (PCA), 10 nM protocatechuate-3,4-dioxygenase (PCD), 1 mM Trolox) (34), and the appropriate experimental nucleotide (5 units ml^{-1} apyrase and no added nucleotides or 2 mM AMP-PNP, or 1 mM –250 nM ATP) was flowed through the chamber. Then a solution containing the kinesin construct to be tested (in buffer A, supplemented with the regeneration, anti-bleaching and appropriate nucleotide) was introduced. Typical concentrations of kinesin protein used in the experiments were ≈ 10 nM for ensemble polarization measurements and ≈ 0.1 nM for the single molecule ones. The flow chamber was then placed in a custom-modified microscope for fluorescence polarization observation and data recording (25).

Fluorescent Polarization Microscopy. Microtubules decorated with the BSR-labeled kinesin constructs were imaged by wide field epifluorescence in a

custom set-up for fluorescence polarization microscopy (25). The laser light excitation ($\lambda = 532$ nm) linear polarization was modulated in 4 different directions (0° , 45° , 90° and 135°) relative to the microscope stage in sync with image acquisition. Images were acquired at a 25 msec/frame rate. Some ensemble polarization data were collected at 100 msec/frame. Ensemble FPM LD⁰ values were estimated as explained in Fig. S1. The order r -factor of single fluorophores and projected angle were calculated as in refs. 20, 25. Time averaged r -factor and projected angles per molecule (Figs. 3 and 4) were calculated by averaging the intensities in all of the frames during the molecule observation time (4 fluorescence intensity averages corresponding to each of the 4 excitation polarization directions). The time-resolved r -factor and projected angle distributions (Fig. 5 B and C) were built using the individual r -factors and projected angles calculated at each 25-msec interval. Time-resolved r -factor traces were obtained by calculating the r -factor using the intensities of 4 contiguous frames. In the time traces (Fig. 5 and Fig. S3), we calculate an r -factor and projected angle every 25 msec using the intensity values obtained from the current frame and the following 3 (4 polarization excitation directions). Thus, the actual time required to calculate 1 data point is 4×25 msec = 100 msec (10 Hz). The Nyquist frequency is half the data acquisition frequency (i.e., 5 Hz) corresponding to a time resolution of 200 msec. The velocity of single kinesin molecules moving processively was determined from kymograph slopes. Low and high r -factor transitions were analyzed using a hidden Markov algorithm as implemented in the program QuB (35). For the analysis, 9 molecules in each experimental condition were chosen based on the shape of the distribution of r -factors. Molecules with broad (approximately bimodal) distributions or r -factors as shown in Fig. 5B were selected. At 1 μM ATP and below, $\approx 40\%$ of all of the molecules investigated fitted this criteria.

ACKNOWLEDGMENTS. We thank M. Tomishige and R.D. Vale for generously providing kinesin DNA plasmids; H. Deng from the Rockefeller University Proteomics Resource Center for mass spectrometry and analysis; A. Stewart, D. Buster, V. DePaoli, D. Sharp, Y. Zhang, and P. Kienker for discussions and critical reading of the manuscript; and E. Perozo and C. Nicolai for suggesting and help using the QuB program. This work was supported by National Institutes of Health Grant RO1-AR48620 (to H.S.).

- Endow SA (2003) Kinesin motors as molecular machines. *Bioessays* 25:1212–1219.
- Svoboda K, Schmidt CF, Schnapp BJ, Block SM (1993) Direct observation of kinesin stepping by optical trapping interferometry. *Nature* 365:721–727.
- Schnitzer MJ, Block SM (1997) Kinesin hydrolyses one ATP per 8-nm step. *Nature* 388:386–390.
- Hua W, Young EC, Fleming ML, Gelles J (1997) Coupling of kinesin steps to ATP hydrolysis. *Nature* 388:390–393.
- Coy DL, Wagenbach M, Howard J (1999) Kinesin takes one 8-nm step for each ATP that it hydrolyzes. *J Biol Chem* 274:3667–3671.
- Rice S, et al. (1999) A structural change in the kinesin motor protein that drives motility. *Nature* 402:778–784.
- Asenjo AB, Weinberg Y, Sosa H (2006) Nucleotide binding and hydrolysis induces a disorder-order transition in the kinesin neck-linker region. *Nat Struct Mol Biol* 13:648–654.
- Tomishige M, Stuurman N, Vale RD (2006) Single-molecule observations of neck linker conformational changes in the kinesin motor protein. *Nat Struct Mol Biol* 13:887–894.
- Howard J, Hudspeth AJ, Vale RD (1989) Movement of microtubules by single kinesin molecules. *Nature* 342:154–158.
- Asbury CL, Fehr AN, Block SM (2003) Kinesin moves by an asymmetric hand-over-hand mechanism. *Science* 302:2130–2134.
- Kasada K, Higuchi H, Hirose K (2003) Alternate fast and slow stepping of a heterodimeric kinesin molecule. *Nat Cell Biol* 5:1079–1082.
- Yildiz A, Tomishige M, Vale RD, Selvin PR (2004) Kinesin walks hand-over-hand. *Science* 303:676–678.
- Hua W, Chung J, Gelles J (2002) Distinguishing inchworm and hand-over-hand processive kinesin movement by neck rotation measurements. *Science* 295:844–848.
- Hackney DD (1994) Evidence for alternating head catalysis by kinesin during microtubule-stimulated Atp hydrolysis. *Proc Natl Acad Sci USA* 91:6865–6869.
- Ma YZ, Taylor EW (1995) Mechanism of microtubule kinesin ATPase. *Biochemistry* 34:13242–13251.
- Gilbert SP, Moyer ML, Johnson KA (1998) Alternating site mechanism of the kinesin ATPase. *Biochemistry* 37:800–813.
- Cross RA, et al. (2000) The conformational cycle of kinesin. *Phil Trans Roy Soc London B* 355:459–464.
- Hackney DD (2007) Biochemistry. Processive motor movement. *Science* 316:58–59.
- Alonso MC, et al. (2007) An ATP gate controls tubulin binding by the tethered head of kinesin-1. *Science* 316:120–123.
- Asenjo AB, Krohn N, Sosa H (2003) Configuration of the two kinesin motor domains during ATP hydrolysis. *Nat Struct Mol Biol* 10:836–842.
- Mori T, Vale RD, Tomishige M (2007) How kinesin waits between steps. *Nature* 450:750–754.
- Kasada K, Higuchi H, Hirose K (2002) Coordination of kinesin's two heads studied with mutant heterodimers. *Proc Natl Acad Sci USA* 99:16058–16063.
- Woehlke G, et al. (1997) Microtubule interaction site of the kinesin motor. *Cell* 90:207–216.
- Crevel IM, Lockhart A, Cross RA (1996) Weak and strong states of kinesin and ncd. *J Mol Biol* 257:66–76.
- Peterman EJ, Sosa H, Goldstein LS, Moerner WE (2001) Polarized fluorescence microscopy of individual and many kinesin motors bound to axonemal microtubules. *Biophys J* 81:2851–2863.
- Hackney DD (2005) The tethered motor domain of a kinesin-microtubule complex catalyzes reversible synthesis of bound ATP. *Proc Natl Acad Sci USA* 102:18338–18343.
- Sosa H, Peterman EJ, Moerner WE, Goldstein LS (2001) ADP-induced rocking of the kinesin motor domain revealed by single-molecule fluorescence polarization microscopy. *Nat Struct Mol Biol* 8:540–544.
- Rice S, et al. (2003) Thermodynamic properties of the kinesin neck-region docking to the catalytic core. *Biophys J* 84:1844–1854.
- Guydosh NR, Block SM (2006) Backsteps induced by nucleotide analogs suggest the front head of kinesin is gated by strain. *Proc Natl Acad Sci USA* 103:8054–8059.
- Rosenfeld SS, Fordyce PM, Jefferson GM, King PH, Block SM (2003) Stepping and stretching. How kinesin uses internal strain to walk processively. *J Biol Chem* 278:18550–18556.
- Yildiz A, Tomishige M, Gennerich A, Vale RD (2008) Intramolecular strain coordinates kinesin stepping behavior along microtubules. *Cell* 134:1030–1041.
- Kapitein LC, et al. (2008) Microtubule cross-linking triggers the directional motility of kinesin-5. *J Cell Biol* 182:421–428.
- Hackney DD, Jiang W (2001) Assays for kinesin microtubule-stimulated ATPase activity. *Methods Mol Biol* 164:65–71.
- Aitken CE, Marshall RA, Puglisi JD (2008) An oxygen scavenging system for improvement of dye stability in single-molecule fluorescence experiments. *Biophys J* 94:1826–1835.
- Qin F (2004) Restoration of single-channel currents using the segmental k-means method based on hidden Markov modeling. *Biophys J* 86:1488–1501.
- Sindelar CV, Downing KH (2007) The beginning of kinesin's force-generating cycle visualized at 9-A resolution. *J Cell Biol* 177:377–385.